Emerging Spin-Orbit Torques in Low-Dimensional Dirac Materials

Joaquín Medina Dueñas,[1,2] José H. García,[1,*] and Stephan Roche[1,3]
[1]ICN2—Catalan Institute of Nanoscience and Nanotechnology, CSIC and BIST, Campus UAB, Bellaterra, 08193 Barcelona, Spain
[2]Department of Physics, Universitat Autònoma de Barcelona (UAB), Campus UAB, Bellaterra, 08193 Barcelona, Spain
[3]ICREA—Institució Catalana de Recerca i Estudis Avançats, 08010 Barcelona, Spain

(Received 3 October 2023; revised 22 April 2024; accepted 3 May 2024; published 25 June 2024)

We report a theoretical description of novel spin-orbit torque components emerging in two-dimensional Dirac materials with broken inversion symmetry. In contrast to usual metallic interfaces where fieldlike and dampinglike torque components are competing, we find that an intrinsic dampinglike torque which derives from all Fermi-sea electrons can be simultaneously enhanced along with the fieldlike component. Additionally, hitherto overlooked torque components unique to Dirac materials emerge from the coupling between spin and pseudospin angular momenta, leading to spin-pseudospin entanglement. These torques are found to be resilient to disorder and could enhance the magnetic switching performance of nearby magnets.

DOI: 10.1103/PhysRevLett.132.266301

Spin-orbit torque (SOT) nonvolatile magnetic memories represent an emerging technology that leverages the intrinsic spin-orbit coupling (SOC) within metals to convert charge current into a spin source, denoted as $\boldsymbol{S}$, further harnessed to manipulate a magnetic state [1,2]. When oriented along unit vector $\hat{\boldsymbol{m}}$, this magnetic state is subjected to a torque $\boldsymbol{T}$ proportional to $\hat{\boldsymbol{m}} \times \boldsymbol{S}$ driving its magnetization dynamics and eventually achieving magnetization reversal [3]. This mechanism offers new possibilities regarding energy efficiency and miniaturization of devices, surpassing traditional multiferromagnet setups [4].

SOT is typically decomposed into two main contributions: the fieldlike (FL) and dampinglike (DL) torques, which respectively cause the magnetization to precess and align along an effective SOC field [3,5,6]. Disentangling these contributions and discerning their respective physical origin has proven to be a long-standing challenge in the field. In conventional metal-magnet interfaces they typically show competing origin, where the FL torque stems from the Rashba-Edelstein effect enabled by the reduced symmetries at the interface, while the DL torque arises from the injection of angular momentum towards the ferromagnet via the spin Hall effect [7,8]. This understanding was called into question by the evidence of strong DL torques in van der Waals heterostructures [9–13] and single-layer devices [14–16], where the spin Hall contribution is suppressed. Intrinsic Berry curvature effects were proposed to originate said torque [14], while skew-scattering mechanisms [17,18] were also proposed as an extrinsic source of DL torque; however, the lack of microscopic information concerning the interface quality does not facilitate a convincing explanation.

The advent of low-dimensional quantum materials opens new avenues for SOT physics. Proximity effects allow for custom charge-to-spin conversion and torque responses [19,20]. Optimal conditions for the Rashba-Edelstein effect were demonstrated for Dirac materials, such as topological surface states [21] and graphene-transition metal dichalcogenide (TMD) bilayers [19,20,22], which can be exploited for SOT applications by proximity effects [18,23–25]. Furthermore, precise control over the system's symmetries enables novel torque responses [26–29] leading to the long-sought-after field-free magnetization switching [30–33].

In this Letter, we develop a general theory for SOT mechanisms in 2D materials, elucidating their microscopic origin rooted in semiclassical or quantum phenomena. To this purpose we combine symmetry analysis, semiclassical modeling, and quantum simulations in realistic electronic models. We first employ group theory to determine the minimal set of torques common to all 2D systems. We then use Boltzmann transport theory to describe the microscopic origin of the emerging torques, and quantify the SOT response using Kubo simulations. We reveal that a DL torque in 2D systems originates from the acceleration of the carriers under spin-momentum locking, and manifests throughout the entire Fermi sea. Furthermore, we find that Dirac materials present hitherto overlooked torque contributions enabled by quantum correlations between spin and pseudospin, which can induce nontrivial magnetization dynamics.

Beyond fieldlike torque in 2D.—We begin by identifying which torque components are allowed by symmetries, beyond the standard FL contribution. We examine nonmagnetic point group $C_{\infty v}$, which represents the highest symmetry group that supports Rashba SOC, exhibiting in-plane axial symmetry and an infinite set of mirror planes perpendicular to the 2D plane, while lacking mirror symmetry parallel to it. Notably, $C_{\infty v}$ encompasses the minimal set of potential torques in 2D systems, as any additional torque can only be enabled by reducing the symmetry group. To determine the minimal set of torques, the nonequilibrium spin density is expressed as a function of the magnetization direction $\hat{\boldsymbol{m}}$ characterized by a polar angle θ, and an azimuthal angle φ relative to the applied electric field $\boldsymbol{\mathcal{E}}$ [see Fig. 1(a), inset]. We retain only the components compatible with the system's symmetries and expand them up to second order in terms of their angular dependence [3,34]. This procedure enables us to separate the nonequilibrium spin density in two contributions, $\boldsymbol{S} = \boldsymbol{S}_{\mathrm{I}} + \boldsymbol{S}_{\mathrm{II}}$, with

$$\boldsymbol{S}_{\mathrm{I}} = \chi_{\mathrm{FL}}(1 - \xi_{\mathrm{FL}}\sin^2\theta)\boldsymbol{H}_{\mathrm{SOC}} - \chi_{\mathrm{DL}}\hat{\boldsymbol{m}} \times \boldsymbol{H}_{\mathrm{SOC}}, \tag{1}$$

corresponding to the standard FL and DL terms, causing the magnetization to precess and align along the effective SOC field $\boldsymbol{H}_{\mathrm{SOC}} \equiv \hat{\boldsymbol{z}} \times \boldsymbol{\mathcal{E}}$. The adimensional parameter ξ_{FL} represents a second order term that modulates the magnetization precession as it approaches the plane. The second contribution reads

$$\boldsymbol{S}_{\mathrm{II}} = -\mathcal{E}(\chi_{\parallel}\cos\varphi + \chi_{\perp}\cos\theta\sin\varphi)\sin\theta\hat{\boldsymbol{z}}, \tag{2}$$

where $\chi_{\parallel}$ generates an anisotropic damping of the in-plane magnetization with respect to the out-of-plane component, while $\chi_{\perp}$ competes with the aforementioned stabilization along $\boldsymbol{H}_{\mathrm{SOC}}$, favoring an alignment parallel or antiparallel

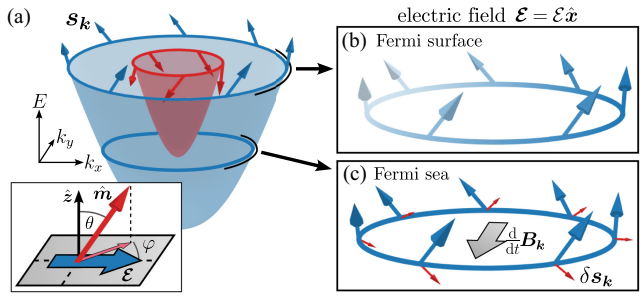

FIG. 1. Physical origin of the FL and DL torques. (a) Spin texture of a 2DEG with Rashba SOC and out-of-plane magnetization ($\theta = 0$). Inset: scheme of the magnetization orientation. When applying an electric field $\boldsymbol{\mathcal{E}}$: (b) the Fermi surface drifts overpopulating states with $\boldsymbol{k} \cdot \boldsymbol{\mathcal{E}} > 0$, generating a nonequilibrium spin density along $\boldsymbol{H}_{\mathrm{SOC}} = \hat{\boldsymbol{z}} \times \boldsymbol{\mathcal{E}}$. (c) The acceleration of the carriers generates a forcing $\sim(d/dt)\boldsymbol{B}_{\boldsymbol{k}}$ (gray). Interaction between the equilibrium spins (blue) and the forcing originates a current-induced spin texture (red), responsible for the DL torque.

to the current depending on the direction of m_z. These torques could be ascertained by observing nontrivial angular dependence in magnetoresistive experiments.

Note that this procedure does not constitute a perturbative expansion. Therefore, these torques, as well as those of higher order, can contribute on equal footing, and their existence and strength will depend on the underlying symmetries and competing fields. To discern their relevance we develop a dual approach. Using the Kubo quantum transport framework, we first determine the nonequilibrium spin density at Fermi level ε_{F} using the Kubo-Bastin formula [35,36],

$$\boldsymbol{S}(\varepsilon_{\mathrm{F}}) = -2\hbar \int d\varepsilon f(\varepsilon)\mathrm{Im}\mathrm{Tr}[\delta(\varepsilon - \hat{H})\hat{\boldsymbol{s}}\partial_{\varepsilon}G^{+}(\hat{\boldsymbol{j}} \cdot \boldsymbol{\mathcal{E}})], \tag{3}$$

where $\hat{H}$, $\hat{\boldsymbol{s}}$, and $\hat{\boldsymbol{j}}$ are the Hamiltonian, spin, and current density operators, respectively, f is the Fermi-Dirac distribution, and $G^{+} = \lim_{\eta\to 0}[\hat{H} - \varepsilon + i\eta]^{-1}$ is the retarded Green's function. Moreover, we distinguish Fermi-sea and Fermi-surface contributions adopting the decomposition proposed in Ref. [37]. We numerically compute Eq. (3) employing a kernel polynomial method (KPM) expansion which includes the choice of a finite energy broadening η [38]. We simulate disordered systems via real-space linear scaling numerical methods, reaching a precision of $\eta \sim$ 15meV in a system with $> 10^6$ orbitals [39–41]. For pristine systems, we develop a k-space KPM calculation of Eq. (3), reaching $\eta \sim 2$ meV precision in systems as large as $> 10^9$ orbitals [41]. To compute $\boldsymbol{S}$ as a function of the magnetization, we select an optimal set of magnetization configurations, each requiring a separate Kubo calculation, resulting in 14 magnetization configurations for each system [41].

Simultaneously, we develop a semiclassical approach based on Boltzmann transport theory to understand the underlying microscopic mechanisms of these torques [43]. Within this theory, the nonequilibrium spin density is

$$\boldsymbol{S}(\varepsilon_{\mathrm{F}}) = \sum_{\mu}\int \frac{d^2\boldsymbol{k}}{(2\pi)^2}[\delta f_{\mu,\boldsymbol{k}}\boldsymbol{s}_{\mu,\boldsymbol{k}} + f(E_{\mu,\boldsymbol{k}})\delta\boldsymbol{s}_{\mu,\boldsymbol{k}}], \tag{4}$$

with $E_{\mu,\boldsymbol{k}}$ and $|E_{\mu,\boldsymbol{k}}\rangle$ the eigenvalue and eigenstate, respectively, of an electron with crystal momentum $\boldsymbol{k}$ and band index μ, and $\boldsymbol{s}_{\mu,\boldsymbol{k}} \equiv \langle E_{\mu,\boldsymbol{k}}|\hat{\boldsymbol{s}}|E_{\mu,\boldsymbol{k}}\rangle$ the mean value of the spin operator $\hat{\boldsymbol{s}}$, commonly referred to as the spin texture. The first term in Eq. (4) represents the standard Boltzmann transport contribution stemming from the current-induced variation of the carrier occupation $\delta f_{\mu,\boldsymbol{k}}$. The origin of the FL torque has been extensively studied and arises from the current-induced drift of the Fermi surface, which combined with the helical spin texture of Rashba systems produces an in-plane spin density perpendicular to the current [44,45], as illustrated in Fig. 1(b).

The second term in Eq. (4) remains less understood. It originates from the adiabatic transport of Bloch states under an electric field and serves as a quantum mechanical correction to the semiclassical result [46]. We here develop an intuitive interpretation of this aspect: as the carriers accelerate in the momentum-dependent Rashba field, a dynamic magnetic field emerges within their rest frame. This field acts as a driving force that nudges the spin away from its equilibrium, producing a current-induced spin texture throughout the entire Fermi sea, as depicted in Fig. 1(c).

To illustrate this point, let us consider a Bloch Hamiltonian that incorporates a spinless component $H_{0,\boldsymbol{k}}$, together with an effective magnetic field $\boldsymbol{B}_{\boldsymbol{k}}$, which encapsulates both the exchange and SOC fields. The Hamiltonian reads $\hat{H}_{\boldsymbol{k}} = H_{0,\boldsymbol{k}} - \frac{1}{2}\boldsymbol{B}_{\boldsymbol{k}} \cdot \hat{\boldsymbol{s}}$ (we take the gyromagnetic ratio equal to unity). In equilibrium, the spin states align along $\boldsymbol{B}_{\boldsymbol{k}}$. When applying an electric field $\boldsymbol{\mathcal{E}}$, the electrons accelerate according to $\hbar(d\boldsymbol{k}/dt) = -e\boldsymbol{\mathcal{E}}$, with e the elementary charge. The spin dynamics emerging from this nonequilibrium state is described by the Ehrenfest theorem, yielding $(d/dt)\boldsymbol{s}_{\mu,\boldsymbol{k}} + \hbar^{-1}\boldsymbol{B}_{\boldsymbol{k}} \times \boldsymbol{s}_{\mu,\boldsymbol{k}} = 0$. We decompose the spin texture into a component aligned with the instantaneous effective field and a perturbation induced by the current: $\boldsymbol{s}_{\mu,\boldsymbol{k}} = \mu\hat{\boldsymbol{B}}_{\boldsymbol{k}} + \delta\boldsymbol{s}_{\mu,\boldsymbol{k}}$, with $\mu = \pm$ indicating the spin majority or minority band respectively. Within the linear response regime, the nonequilibrium spin texture reads

$$\delta\boldsymbol{s}_{\mu,\boldsymbol{k}} = -\mu\frac{e\hbar}{B_{\boldsymbol{k}}^3}\boldsymbol{B}_{\boldsymbol{k}} \times (\boldsymbol{\mathcal{E}} \cdot \nabla_{\boldsymbol{k}})\boldsymbol{B}_{\boldsymbol{k}}. \tag{5}$$

This result reveals a crucial point: the interplay between the equilibrium and dynamic magnetic fields results in a current-induced shift of the spin texture. Notably, this nonequilibrium spin texture component is the main contributor to the DL torque observed in 2D magnetic Rashba systems, revealing its semiclassical nature.

Semiclassical torque mechanisms in a 2D electron gas.—To highlight our theory's capabilities, we begin by demonstrating the existence of a DL torque in an s-wave 2D electron gas (2DEG) with $C_{\infty v}$ symmetry, generated by the proposed semiclassical mechanism. The magnetization is characterized by an exchange splitting J_{ex} along the magnetization direction $\hat{\boldsymbol{m}}$, while the Rashba SOC field is helical with an isotropic amplitude $\Lambda_{\mathrm{R},k}$. The Hamiltonian is $\hat{H}_{\boldsymbol{k}} = H_{0,k} - \frac{1}{2}\Lambda_{\mathrm{R},k}\hat{\boldsymbol{\varphi}} \cdot \hat{\boldsymbol{s}} - \frac{1}{2}J_{\mathrm{ex}}\hat{\boldsymbol{m}} \cdot \hat{\boldsymbol{s}}$, with $H_{0,k}$ the kinetic term, and $\hat{\boldsymbol{\varphi}} = \hat{\boldsymbol{z}} \times \hat{\boldsymbol{k}}$. We determine the nonequilibrium spin density employing Boltzmann transport assuming an isotropic momentum relaxation time τ in the weak disorder regime. A perturbative expansion in terms of the magnetization direction is appropriate only if the effective magnetic field is dominated either by the exchange or Rashba term. We begin by defining the leading order effective magnetic field, $B_{0,k} = (J_{\mathrm{ex}}^2 + \Lambda_{\mathrm{R},k}^2)^{1/2}$, isotropic in momentum space. For a dominant exchange splitting, which is usually the experimental condition, $B_0 \approx J_{\mathrm{ex}}$ is momentum independent, while for a dominant Rashba splitting $B_{0,k} \approx \Lambda_{\mathrm{R},k}$.

The conventional torques, represented in $\boldsymbol{S}_{\mathrm{I}}$, show a similar behavior in both regimes. The FL torque is essentially determined by the spin helicity, $\boldsymbol{s}_{\mu,\boldsymbol{k}} \cdot \hat{\boldsymbol{\varphi}} \approx \mu\Lambda_{\mathrm{R},k}/B_{0,k}$. It derives from the Fermi-surface contribution to Eq. (4), and is proportional to the density of states and the electron mobility following

$$\chi_{\mathrm{FL},\mu} = \mu\frac{e\tau k_\mu}{4\pi\hbar}\frac{\Lambda_{\mathrm{R},k_\mu}}{B_{0,k_\mu}}, \tag{6}$$

where $\chi_{\mathrm{FL},\mu}$ is the FL torque response for band μ, with $\mu = \pm$. The electron mobility is contained within τ, and k_μ is the isotropic part of the Fermi momentum, which encodes the density of states, defined such that $\varepsilon_{\mathrm{F}} = H_{0,k_\mu} - (\mu/2)B_{0,k_\mu}$.

The DL torque on the other hand, is determined by the Fermi-sea integral of the current-induced spin texture $\delta\boldsymbol{s}_{\mu,\boldsymbol{k}}$. $\delta\boldsymbol{s}_{\mu,\boldsymbol{k}}$ emerges from the interaction between the equilibrium spin texture, and the variation of the effective magnetic field in the accelerating electron rest frame via spin-momentum locking, as given by Eq. (5). Only the Rashba field $\Lambda_{\mathrm{R},k}\hat{\boldsymbol{\varphi}}$ contributes to the latter, yielding $\int d\varphi(\boldsymbol{\mathcal{E}} \cdot \nabla_{\boldsymbol{k}})\boldsymbol{B}_{\boldsymbol{k}} = (\pi/k)\partial_k(k\Lambda_{\mathrm{R},k})\boldsymbol{H}_{\mathrm{SOC}}$, whose interaction with the spin texture component parallel to the magnetization $\hat{\boldsymbol{m}}$ generates the DL torque

$$\chi_{\mathrm{DL},\mu} = \mu\frac{eJ_{\mathrm{ex}}}{4\pi}\int_0^{k_\mu} dk\,\frac{\partial_k(k\Lambda_{\mathrm{R},k})}{B_{0,k}^3}, \tag{7}$$

with $\chi_{\mathrm{DL},\mu}$ the DL torque response for band μ. This expression reveals that the DL torque is generated by the interplay between spin-momentum locking and exchange splitting throughout the entire Fermi sea. In the particular case of a dominant exchange splitting the effective field is momentum independent, and the DL torque becomes $\chi_{\mathrm{DL}} = (\hbar/\tau J_{\mathrm{ex}})\chi_{\mathrm{FL}}$, thus offering a way to determine the momentum relaxation time via the $\chi_{\mathrm{FL}}/\chi_{\mathrm{DL}}$ ratio. Additionally, the interaction between the dynamic magnetic field and the equilibrium Rashba field produces an out-of-plane current-induced spin density inducing an unconventional torque $\chi_{\parallel}$, which is only nonzero in the Rashba dominated regime [41].

We find that the second order torques vanish in parabolic systems, $\chi_{\perp} = \xi_{\mathrm{FL}} = 0$. In the exchange dominated regime, the spin texture presents a dominant component aligned with $\hat{\boldsymbol{m}}$, while Rashba SOC introduces a helical component as well as an anisotropic modulation to the dominating one. Hence, the drift of the Fermi surface, in addition to the FL torque, also yields a nonequilibrium spin density parallel to the magnetization, which stems from the spin texture component parallel to $\hat{\boldsymbol{m}}$ and cannot exert any torque,

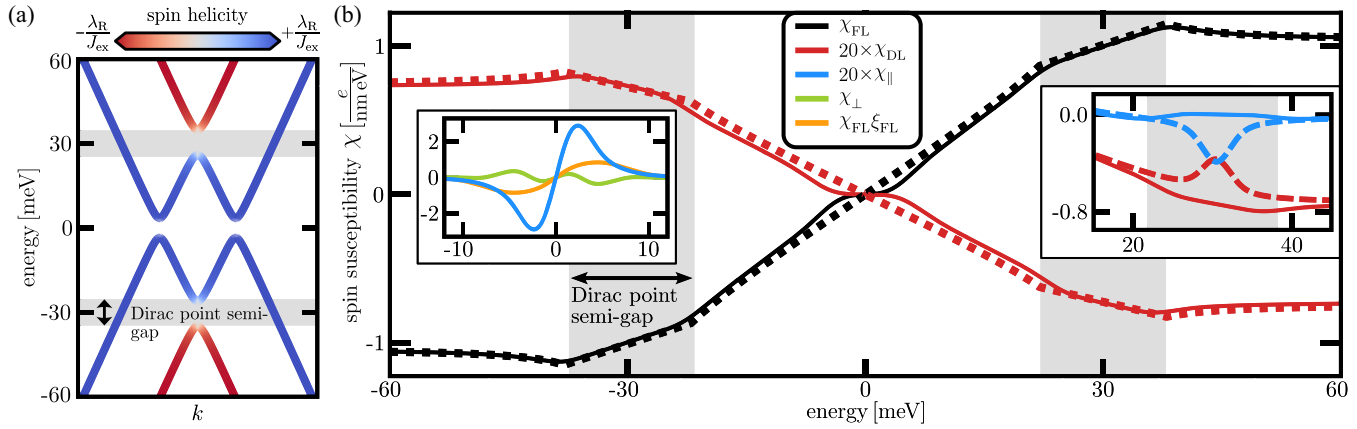

FIG. 2. SOT in Dirac matter. (a) Band structure of Dirac system with Rashba SOC and exchange splitting [$\theta = 0$]. (b) The conventional SOTs, χ_{FL} and χ_{DL}, are driven by semiclassical effects, evinced by the agreement between semiclassical (dotted curves) and Kubo-Bastin (solid curves) frameworks. The insets show torque responses, computed by the Kubo framework, which are not captured by semiclassical effects. Left inset: all unconventional torques show a strong enhancement near the band inversion at charge neutrality. Right inset: χ_{DL} and $\chi_{\parallel}$ shift from semiclassical to quantum-driven mechanisms at the Dirac point, as the semigap is dominated by the effective mass ($\Delta \neq 0$, solid curves) or Rashba SOC ($\Delta = 0$, dashed curves), respectively. ($v \sim 10^6$ m/s, $\lambda_R = 8$ meV, $J_{ex} = 60$ meV, $\Delta = 8$ meV, $\eta = 2$ meV at the band center and $\tau = \hbar/\eta$, except if indicated otherwise.).

but could be relevant in multiferromagnet configurations, as emerging in the anomalous spin Hall effect [41,47–51]. Finally, we demonstrate that our theory fully matches quantum simulations for the description of DL torque in an s-wave 2DEG [41].

Unconventional torques in Dirac matter.—We now use our theory to reveal unconventional torques in Dirac systems enabled by quantum correlations between the spin and the additional angular momentum degree of freedom provided by the pseudospin. We consider a Dirac Hamiltonian of non-magnetic point group symmetry $C_{\infty v}$ doted with exchange splitting, given by $\hat{H}_{\boldsymbol{k}} = \hbar v \boldsymbol{k}\cdot\hat{\boldsymbol{\sigma}} + \Delta\sigma_z - \frac{1}{2}\lambda_R(\hat{\boldsymbol{s}}\times\hat{\boldsymbol{\sigma}})\cdot\hat{\boldsymbol{z}} - \frac{1}{2}J_{ex}\hat{\boldsymbol{m}}\cdot\hat{\boldsymbol{s}}$, with v the velocity of massless Dirac electrons, Δ their effective mass, and λ_R the Rashba SOC parameter, while the pseudospin is represented by Pauli vector $\hat{\boldsymbol{\sigma}}$. Such a system may be realized by an insulating ferromagnet-graphene-TMD trilayer [18], where proximity effects induce SOC and exchange splitting [52–54]. Rashba splitting in graphene-TMD interfaces is typically of order $\sim$1 meV [55–58], while proximity with a ferromagnet can reach exchange splittings as large as $\sim$100 meV [59,60]. We thus focus on the regime with a dominant exchange splitting.

Spin-momentum locking in Dirac electrons is mediated by the pseudospin. The 2DEG paradigm may be recovered in absence of spin-pseudospin correlations, i.e., $\langle\sigma_i s_j\rangle = \langle\sigma_i\rangle\langle s_j\rangle$, allowing us to define an effective Rashba field for each pseudospin polarized set of bands. This is the case far from band crossings, where Rashba SOC perturbatively imprints a helical component to the spin texture. Drastically different is the situation near band crossings, where Rashba SOC acts nonperturbatively by hybridizing bands of opposite pseudospin polarizations, while also inducing non-negligible spin-pseudospin correlations. These two regimes must be analyzed separately.

In the former regime, the pair of bands with opposite pseudospin polarization, or equivalently, opposite velocities, are decoupled. We thus recover the 2DEG paradigm by adequately adjusting for the corresponding kinetic Hamiltonian and Rashba field, allowing us to understand the FL and DL torques from simple band structure properties, shown in Fig. 2(a): At energies larger than the magnetic splitting the spectrum presents two Fermi contours with positive velocity which compete due to their opposite helicities. Such competition is energy independent due to the linear dispersion. For energies lower than the magnetic splitting, the two Fermi contours present the same helicity, but with opposite velocity. The inner Fermi contour vanishes when approaching the spin-split Dirac point, where Δ opens a semigap. Within the semigapped energy window a single spin-helical band remains, representing an optimal condition for maximizing the SOT efficiency. The semiclassical results are in very good agreement with Kubo calculations, as shown in Fig. 2(b). Additionally, we recover the previously obtained relation for the momentum relaxation time and the torque ratio, $\tau = (\hbar/J_{ex})\chi_{FL}/\chi_{DL}$.

Near the band inversion at charge neutrality the hybridization between bands of opposite velocity breaks the 2DEG paradigm. To elucidate the torques in this regime, the full quantum response provided by the Kubo-Bastin formula is required. The results are shown in the left inset of Fig. 2(b), where strong unconventional torques are seen near the Rashba gap, vanishing in the 2DEG case. The origin of these torques is twofold. Despite the dominant exchange splitting, Rashba SOC acts nonperturbatively and induces strong anisotropies in the dispersion. Furthermore, non-negligible spin-pseudospin correlations quench the spin

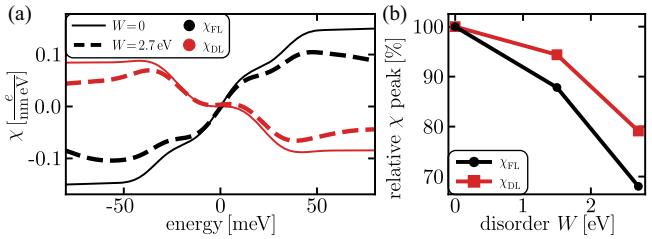

FIG. 3. The FL and DL torques are robust against Anderson disorder (of strength W). (a) SOT for pristine (solid) and $W = 2.7$ eV disordered (dashed) systems. (b) Peak torque values relative to the pristine system. ($v \sim 10^6$ m/s, $\lambda_R = 10$ meV, $J_{ex} = 40$ meV, $\Delta = 5$ meV, and $\eta = 15$ meV at the band center).

texture [61–63] and modify the coupled spin-pseudospin dynamics [41]. These two features are only possible due to the additional pseudospin degree of freedom.

At the Dirac point, the SOT physics may shift from semiclassical to quantum driven effects. While the effective mass Δ acts separately on each spin-split Dirac cone, Rashba SOC couples them favoring spin-pseudospin entanglement [61,62]. At the spin-split Dirac point the spectrum is semigapped, thus transport should be dominated by the band of the opposite cone, whose physics is mainly determined by the kinetic term of the Hamiltonian, insensitive to Δ. This is indeed the case for massive Dirac electrons, as shown in Fig. 2(b), right inset (solid curves), where $|\chi_{DL}|$ increases across the semigap while $\chi_{\parallel}$ remains negligible. However, the torques change dramatically for massless electrons, as $|\chi_{DL}|$ is minimal and $|\chi_{\parallel}|$ peaks within the semigap, shown in Fig. 2(b), right inset (dashed curves). This qualitative change is generated due to spin-pseudospin entanglement dominating the gap, indicating a large torque originated from a vanishing Fermi contour.

Finally, we compute the Kubo-Bastin response considering real-space Anderson disorder of strength W [39–41]. Real-space simulations heavily increase the computational cost, which results in a coarser energy broadening with respect to previous calculations. The results are shown in Fig. 3, focusing on the FL and DL torques. For W as high as 2.7 eV, the χ_{FL} and χ_{DL} peaks are only reduced to 68% and 79% of their respective pristine values. Dictated by a Fermi-sea contribution, χ_{DL} shows a better resilience than χ_{FL}.

In conclusion, we developed a general theory for SOT in 2D materials, elucidating the nature of the subjacent physical mechanisms. Novel torque components were found to emerge and superimpose, where quantum spin-pseudospin correlations in Dirac electrons yield nontrivial SOT phenomena. This conclusion is expected to be general to systems where spin-momentum locking is mediated by additional degrees of freedom, as can also occur with orbital angular momentum [64]. Our findings provide guidelines for enhancing the torque capability of low-dimensional systems, allowing further exploration of energy-efficient memory technologies.

The authors thank D. García Ovalle and A. Manchon for fruitful discussions. The authors acknowledge funding from the project I+D+i PID2022-138283NB-I00 funded by MICIU/AEI/10.13039/501100011033/ and "FEDER Una manera de hacer Europa," FLAG-ERA project MNEMOSYN (PCI2021-122035-2A) funded by MICIU/AEI/10.13039/501100011033 and the European Union NextGenerationEU/PRTR, and ERC project AI4SPIN funded by the European Union's Horizon Europe research and innovation programme—European Research Council Executive Agency under Grant Agreement No. 101078370-AI4SPIN. J. M. D. acknowledges support from MICIU Grant No. FPI PRE2021-097031. S. R. acknowledges support from 2021 SGR 00997, funded by Generalitat de Catalunya. ICN2 is funded by the CERCA Programme/Generalitat de Catalunya and supported by the Severo Ochoa Centres of Excellence programme, Grant No. CEX2021-001214-S, funded by MCIN/AEI/10.13039.501100011033.

*Corresponding author: josehugo.garcia@icn2.cat

[1] K. Ando, S. Takahashi, K. Harii, K. Sasage, J. Ieda, S. Maekawa, and E. Saitoh, Electric manipulation of spin relaxation using the spin Hall effect, Phys. Rev. Lett. **101**, 036601 (2008).

[2] I. M. Miron, G. Gaudin, S. Auffret, B. Rodmacq, A. Schuhl, S. Pizzini, J. Vogel, and P. Gambardella, Current-driven spin torque induced by the Rashba effect in a ferromagnetic metal layer, Nat. Mater. **9**, 230 (2010).

[3] A. Manchon, J. Železný, I. M. Miron, T. Jungwirth, J. Sinova, A. Thiaville, K. Garello, and P. Gambardella, Current-induced spin-orbit torques in ferromagnetic and antiferromagnetic systems, Rev. Mod. Phys. **91**, 035004 (2019).

[4] H. Yang, S. O. Valenzuela, M. Chshiev, S. Couet, B. Dieny, B. Dlubak, A. Fert, K. Garello, M. Jamet, D.-E. Jeong, K. Lee, T. Lee, M.-B. Martin, G. S. Kar, P. Sénéor, H.-J. Shin, and S. Roche, Two-dimensional materials prospects for non-volatile spintronic memories, Nature (London) **606**, 663 (2022).

[5] P. M. Haney, H.-W. Lee, K.-J. Lee, A. Manchon, and M. D. Stiles, Current induced torques and interfacial spin-orbit coupling: Semiclassical modeling, Phys. Rev. B **87**, 174411 (2013).

[6] R. Ramaswamy, J. M. Lee, K. Cai, and H. Yang, Recent advances in spin-orbit torques: Moving towards device applications, Appl. Phys. Rev. **5**, 031107 (2018).

[7] J. Kim, J. Sinha, M. Hayashi, M. Yamanouchi, S. Fukami, T. Suzuki, S. Mitani, and H. Ohno, Layer thickness dependence of the current-induced effective field vector in Ta|CoFeB|MgO, Nat. Mater. **12**, 240 (2013).

[8] R. Ramaswamy, X. Qiu, T. Dutta, S. D. Pollard, and H. Yang, Hf thickness dependence of spin-orbit torques in Hf/CoFeB/MgO heterostructures, Appl. Phys. Lett. **108**, 202406 (2016).

[9] W. Zhang, J. Sklenar, B. Hsu, W. Jiang, M. B. Jungfleisch, J. Xiao, F. Y. Fradin, Y. Liu, J. E. Pearson, J. B. Ketterson, Z. Yang, and A. Hoffmann, Research Update: Spin transfer

torques in permalloy on monolayer MoS2, APL Mater. **4**, 032302 (2016).
[10] D. MacNeill, G. M. Stiehl, M. H. D. Guimaraes, R. A. Buhrman, J. Park, and D. C. Ralph, Control of spin–orbit torques through crystal symmetry in WTe2/ferromagnet bilayers, Nat. Phys. **13**, 300 (2017).
[11] W. Lv, Z. Jia, B. Wang, Y. Lu, X. Luo, B. Zhang, Z. Zeng, and Z. Liu, Electric-field control of spin–orbit torques in WS2/permalloy bilayers, ACS Appl. Mater. Interfaces **10**, 2843 (2018).
[12] H. Kurebayashi, J. H. García, S. Khan, J. Sinova, and S. Roche, Magnetism, symmetry and spin transport in van der Waals layered systems, Nat. Rev. Phys. **4**, 150 (2022).
[13] J. Hidding, K. Mërtiri, F. Mujid, C. Liang, J. Park, and M. H. D. Guimarães, Role of self-torques in transition metal dichalcogenide/ferromagnet bilayers, Phys. Rev. B **108**, 064419 (2023).
[14] H. Kurebayashi, J. Sinova, D. Fang, A. C. Irvine, T. D. Skinner, J. Wunderlich, V. Novák, R. P. Campion, B. L. Gallagher, E. K. Vehstedt, L. P. Zârbo, K. Výborný, A. J. Ferguson, and T. Jungwirth, An antidamping spin–orbit torque originating from the Berry curvature, Nat. Nanotechnol. **9**, 211 (2014).
[15] T. Seki, Y.-C. Lau, S. Iihama, and K. Takanashi, Spin-orbit torque in a Ni-Fe single layer, Phys. Rev. B **104**, 094430 (2021).
[16] M. Aoki, Y. Yin, S. Granville, Y. Zhang, N. V. Medhekar, L. Leiva, R. Ohshima, Y. Ando, and M. Shiraishi, Gigantic anisotropy of self-induced spin-orbit torque in Weyl ferromagnet Co2MnGa, Nano Lett. **23**, 6951 (2023).
[17] F. Sousa, G. Tatara, and A. Ferreira, Skew-scattering-induced giant antidamping spin-orbit torques: Collinear and out-of-plane Edelstein effects at two-dimensional material/ferromagnet interfaces, Phys. Rev. Res. **2**, 043401 (2020).
[18] K. Zollner, M. D. Petrović, K. Dolui, P. Plecháč, B. K. Nikolić, and J. Fabian, Scattering-induced and highly tunable by gate damping-like spin-orbit torque in graphene doubly proximitized by two-dimensional magnet $Cr_2Ge_2Te_6$ and monolayer WS_2, Phys. Rev. Res. **2**, 043057 (2020).
[19] L. A. Benítez, W. S. Torres, J. F. Sierra, M. Timmermans, J. H. García, S. Roche, M. V. Costache, and S. O. Valenzuela, Tunable room-temperature spin galvanic and spin Hall effects in van der Waals heterostructures, Nat. Mater. **19**, 170 (2020).
[20] A. M. Hoque, D. Khokhriakov, K. Zollner, B. Zhao, B. Karpiak, J. Fabian, and S. P. Dash, All-electrical creation and control of spin-galvanic signal in graphene and molybdenum ditelluride heterostructures at room temperature, Commun. Phys. **4**, 124 (2021).
[21] D. Pesin and A. H. MacDonald, Spintronics and pseudospintronics in graphene and topological insulators, Nat. Mater. **11**, 409 (2012).
[22] M. Offidani, M. Milletarì, R. Raimondi, and A. Ferreira, Optimal charge-to-spin conversion in graphene on transition-metal dichalcogenides, Phys. Rev. Lett. **119**, 196801 (2017).
[23] I. Garate and M. Franz, Inverse spin-galvanic effect in the interface between a topological insulator and a ferromagnet, Phys. Rev. Lett. **104**, 146802 (2010).
[24] A. R. Mellnik, J. S. Lee, A. Richardella, J. L. Grab, P. J. Mintun, M. H. Fischer, A. Vaezi, A. Manchon, E.-A. Kim, N. Samarth, and D. C. Ralph, Spin-transfer torque generated by a topological insulator, Nature (London) **511**, 449 (2014).
[25] S. Ghosh and A. Manchon, Spin-orbit torque in a three-dimensional topological insulator–ferromagnet heterostructure: Crossover between bulk and surface transport, Phys. Rev. B **97**, 134402 (2018).
[26] S. Fukami, C. Zhang, S. DuttaGupta, A. Kurenkov, and H. Ohno, Magnetization switching by spin–orbit torque in an antiferromagnet–ferromagnet bilayer system, Nat. Mater. **15**, 535 (2016).
[27] O. Johansen, V. Risinggard, A. Sudbo, J. Linder, and A. Brataas, Current control of magnetism in two-dimensional Fe_3GeTe_2, Phys. Rev. Lett. **122**, 217203 (2019).
[28] A. F. May, M.-H. Du, V. R. Cooper, and M. A. McGuire, Tuning magnetic order in the van der Waals metal Fe_5GeTe_2 by cobalt substitution, Phys. Rev. Mater. **4**, 074008 (2020).
[29] A. Roy, M. H. D. Guimarães, and J. Sławińska, Unconventional spin Hall effects in nonmagnetic solids, Phys. Rev. Mater. **6**, 045004 (2022).
[30] M. Jiang, H. Asahara, S. Sato, T. Kanaki, H. Yamasaki, S. Ohya, and M. Tanaka, Efficient full spin–orbit torque switching in a single layer of a perpendicularly magnetized single-crystalline ferromagnet, Nat. Commun. **10**, 2590 (2019).
[31] L. Liu, C. Zhou, X. Shu, C. Li, T. Zhao, W. Lin, J. Deng, Q. Xie, S. Chen, J. Zhou, R. Guo, H. Wang, J. Yu, S. Shi, P. Yang, S. Pennycook, A. Manchon, and J. Chen, Symmetry-dependent field-free switching of perpendicular magnetization, Nat. Nanotechnol. **16**, 277 (2021).
[32] L. Liu, C. Zhou, T. Zhao, B. Yao, J. Zhou, X. Shu, S. Chen, S. Shi, S. Xi, D. Lan, W. Lin, Q. Xie, L. Ren, Z. Luo, C. Sun, P. Yang, E.-J. Guo, Z. Dong, A. Manchon, and J. Chen, Current-induced self-switching of perpendicular magnetization in CoPt single layer, Nat. Commun. **13**, 3539 (2022).
[33] B. Zhao, L. Bainsla, R. Ngaloy, P. Svedlindh, and S. P. Dash, Coexistence of non-trivial van der Waals magnetic orders enable field-free spin-orbit torque switching at room temperature, arXiv:2308.13408.
[34] D. García Ovalle, A. Pezo, and A. Manchon, Spin-orbit torque for field-free switching in C_{3v} crystals, Phys. Rev. B **107**, 094422 (2023).
[35] R. Kubo, Statistical-mechanical theory of irreversible processes. I. General theory and simple applications to magnetic and conduction problems, J. Phys. Soc. Jpn. **12**, 570 (1957).
[36] A. Bastin, C. Lewiner, O. Betbeder-matibet, and P. Nozieres, Quantum oscillations of the Hall effect of a fermion gas with random impurity scattering, J. Phys. Chem. Solids **32**, 1811 (1971).
[37] V. Bonbien and A. Manchon, Symmetrized decomposition of the Kubo-Bastin formula, Phys. Rev. B **102**, 085113 (2020).
[38] A. Weisse, G. Wellein, A. Alvermann, and H. Fehske, The kernel polynomial method, Rev. Mod. Phys. **78**, 275 (2006).
[39] J. H. García, L. Covaci, and T. G. Rappoport, Real-space calculation of the conductivity tensor for disordered topological matter, Phys. Rev. Lett. **114**, 116602 (2015).
[40] Z. Fan, J. H. García, A. W. Cummings, J. E. Barrios-Vargas, M. Panhans, A. Harju, F. Ortmann, and S. Roche, Linear scaling quantum transport methodologies, Phys. Rep. **903**, 1 (2021).

[41] See Supplemental Material at http://link.aps.org/supplemental/10.1103/PhysRevLett.132.266301 for details on Kubo-Bastin simulations and semiclassical SOT calculations, which additionally includes Ref. [42].
[42] W. K. Wootters, Entanglement of formation of an arbitrary state of two qubits, Phys. Rev. Lett. **80**, 2245 (1998).
[43] N. A. Sinitsyn, Semiclassical theories of the anomalous Hall effect, J. Phys. Condens. Matter **20**, 023201 (2007).
[44] V. M. Edelstein, Spin polarization of conduction electrons induced by electric current in two-dimensional asymmetric electron systems, Solid State Commun. **73**, 233 (1990).
[45] A. Manchon and S. Zhang, Theory of nonequilibrium intrinsic spin torque in a single nanomagnet, Phys. Rev. B **78**, 212405 (2008).
[46] D. Xiao, M.-C. Chang, and Q. Niu, Berry phase effects on electronic properties, Rev. Mod. Phys. **82**, 1959 (2010).
[47] T. Taniguchi, J. Grollier, and M. D. Stiles, Spin-transfer torques generated by the anomalous Hall effect and anisotropic magnetoresistance, Phys. Rev. Appl. **3**, 044001 (2015).
[48] K. S. Das, W. Y. Schoemaker, B. J. van Wees, and I. J. Vera-Marun, Spin injection and detection via the anomalous spin Hall effect of a ferromagnetic metal, Phys. Rev. B **96**, 220408(R) (2017).
[49] S. Iihama, T. Taniguchi, K. Yakushiji, A. Fukushima, Y. Shiota, S. Tsunegi, R. Hiramatsu, S. Yuasa, Y. Suzuki, and H. Kubota, Spin-transfer torque induced by the spin anomalous Hall effect, National electronics review **1**, 120 (2018).
[50] J. D. Gibbons, D. MacNeill, R. A. Buhrman, and D. C. Ralph, Reorientable spin direction for spin current produced by the anomalous Hall effect, Phys. Rev. Appl. **9**, 064033 (2018).
[51] V. P. Amin, J. Li, M. D. Stiles, and P. M. Haney, Intrinsic spin currents in ferromagnets, Phys. Rev. B **99**, 220405(R) (2019).
[52] S. Konschuh, M. Gmitra, and J. Fabian, Tight-binding theory of the spin-orbit coupling in graphene, Phys. Rev. B **82**, 245412 (2010).
[53] M. Gmitra and J. Fabian, Graphene on transition-metal dichalcogenides: A platform for proximity spin-orbit physics and optospintronics, Phys. Rev. B **92**, 155403 (2015).
[54] J. C. Leutenantsmeyer, A. A. Kaverzin, M. Wojtaszek, and B. J. v. Wees, Proximity induced room temperature ferromagnetism in graphene probed with spin currents, 2D Mater. **4**, 014001 (2016).
[55] A. Avsar, J. Y. Tan, T. Taychatanapat, J. Balakrishnan, G. K. W. Koon, Y. Yeo, J. Lahiri, A. Carvalho, A. S. Rodin, E. C. T. O'Farrell, G. Eda, A. H. Castro Neto, and B. Özyilmaz, Spin–orbit proximity effect in graphene, Nat. Commun. **5**, 4875 (2014).
[56] Z. Wang, D.-K. Ki, H. Chen, H. Berger, A. H. MacDonald, and A. F. Morpurgo, Strong interface-induced spin–orbit interaction in graphene on WS_2, Nat. Commun. **6**, 8339 (2015).
[57] Y. Li and M. Koshino, Twist-angle dependence of the proximity spin-orbit coupling in graphene on transition-metal dichalcogenides, Phys. Rev. B **99**, 075438 (2019).
[58] T. Naimer, K. Zollner, M. Gmitra, and J. Fabian, Twist-angle dependent proximity induced spin-orbit coupling in graphene/transition metal dichalcogenide heterostructures, Phys. Rev. B **104**, 195156 (2021).
[59] A. Hallal, F. Ibrahim, H. Yang, S. Roche, and M. Chshiev, Tailoring magnetic insulator proximity effects in graphene: First-principles calculations, 2D Mater. **4**, 025074 (2017).
[60] F. Ibrahim, A. Hallal, D. S. Lerma, X. Waintal, E. Y. Tsymbal, and M. Chshiev, Unveiling multiferroic proximity effect in graphene, 2D Mater. **7**, 015020 (2019).
[61] D. V. Tuan, F. Ortmann, D. Soriano, S. O. Valenzuela, and S. Roche, Pseudospin-driven spin relaxation mechanism in graphene, Nat. Phys. **10**, 857 (2014).
[62] B. G. de Moraes, A. W. Cummings, and S. Roche, Emergence of intraparticle entanglement and time-varying violation of Bell's inequality in Dirac matter, Phys. Rev. B **102**, 041403(R) (2020).
[63] J. Martínez Romeral, A. W. Cummings, and S. Roche, Resilient intraparticle entanglement and its manifestation in spin dynamics of disordered Dirac matter, arXiv:2310.17950.
[64] D. Go, D. Jo, C. Kim, and H.-W. Lee, Intrinsic spin and orbital Hall effects from orbital texture, Phys. Rev. Lett. **121**, 086602 (2018).